Supporting Information

1. DETAILED DESCRIPTION OF MATERIALS SAMPLING AND METHODS

1.1. Location of the Mill and Milling Process

The Key Lake U mill (57°13′N, 105°38′W) and the Deilmann TMF (DTMF) into which its tailings are discharged were selected for study due to the presence of ferrihydrite in the mill and tailings being well documented and shown to control the solubility of EOCs. The mill started operations in 1983 and, based on known reserves, is expected to continue operating to 2040. As of October 2009, the mill had produced more than ~170 million kg of U_3O_8. The production at the mill currently accounts for 16% of the world's annual U production and is currently the world's largest high-grade U-milling operation.[2, 20-21]

The Key Lake mill uses a strong acid (H_2SO_4) digestion process in conjunction with strong oxidizing conditions (target Eh = +600 mV) to leach U from the ore. These conditions also oxidize metal sulphides and arsenides and liberate metalloids and metals including As, Ni, Mo, and Se from the ore. Once solubilized, the U is stripped from the acidic leachate using a solvent extraction process. The remaining aqueous phase (raffinate) reports to a series of four neutralization tanks (pachucas) where hydrated lime is added in stages to increase the pH from 1.0 to 3.5, to 4.2, to 6.5, and finally 9.2 (Figure S0). The overflow from the second pachuca feeds into the selenium-molybdenum (Se-Mo) thickener for precipitation. The secondary minerals in the slurry are thickened to 25% solids and neutralized to pH 7.0 before reporting as underflow to the discharging tailings. The supernatant of the Se-Mo thickener overflows into Pachuca 3. The slurry from the final pachuca (pH

9.2) is thickened in the lamella thickner before reporting to the final tailings thickener where flocculent is added and the leach residue (the unleached ore collected from the counter decantation leach circuit) and Mo-Se removal streams are recombined. Finally, lime is added to increase the final tailings discharge pH to approximately 10.5. Since July 2002, $BaCl_2$ has been added to the pachucas to reduce the dissolved ^{226}Ra concentration during neutralization. A radium removal thickener installed at the terminus of the system serves to remove final precipitates that make up a minor contribution to the final tailings.[22]

1.2 Deilmann Tailings Management Facility

Tailings generated in the mill have been deposited in the DTMF, a mined out pit, since 1996. Between 1996 and 1999, the mill feed was derived entirely from the polymetallic U-Ni Deilmann ore body containing varying amounts of Ni-Co-As-S, minerals. Since 1999, ore from the McArthur River mine, located 80 km north of the Key Lake mill, has been the primary source of ore for the mill.[23-24] This ore is mixed with varying amounts of lower grade ores and waste materials from Key Lake and McArthur River mines. In general, the McArthur River ores are high-grade U ore bodies containing significantly lesser amounts of Ni-Co-As-S sulfide minerals than the Deilmann ore body. The difference in EOC concentrations in the ores is reflected in the tailings. Shaw et al.[6] show that the DTMF body can be divided into two geochemical layers: deeper tailings (at elevation < 410 m above sea level (masl)) mostly generated from the Deilmann ore and overlying tailings (at elevation > 410 masl) from the McArthur River ore. The Deilmann tailings solids are generally characterized by greater elemental concentrations than the McArthur River tailings, particularly As, Co, and Ni. Mean E_h values measured on extracted porewaters from the Deilmann and McArthur River tailings are between +193 to +206 mV[6], indicating that oxic conditions exist in the tailings and have existed since deposition.

2.3. Sample Collection and Preparation

Composite samples of secondary precipitates generated in the raffinate neutralization process were collected in August 2011 to compare the mineral phases present in the neutralized raffinate to those in the tailings. Slurries from the pachucas and thickeners were collected along the neutralization process at pH 1.4 (unbuffered raffinate), 4.3, 4.4, 6.5, and 10.1 (Figure 1, Table 2). These were termed 11-KL-01 to 11-KL-05, respectively (note the 11-KL-01 sample contained only an aqueous phase).

Samples were also collected from the underflows from the Se-Mo thickener and the lamella thickener (see sampling points A and B; Figure 1). These samples were mixed at a 1:1 volume ratio to replicate the composite discharge from the mill. The composite sample was amended with slaked lime (to a terminal pH of 11) and barium chloride (sample termed 11-CS-Ba). A second composite sample (termed 11-CS-OO) was collected in September 2011 in the same manner as described above. It was also treated with slaked lime but no barium chloride was added to simplify our XRD phase analysis (i.e. No $BaSO_4$). Samples were stirred for 8 h to ensure stabilization at pH 11, then an aliquot (1 L volume) of each collected for analysis. Due to the similarity between these two data sets (i.e., 11-CS-OO and 11-CS-Ba), only the data from 11-CS-Ba are presented.

In addition to the neutralized samples from the underflows from the Se-Mo thickener and the lamella thickener, three tailings samples were collected for analysis. The first tailings sample, generated from McArthur River ore (11-McTail-01), was collected in September 2011 from the final tailings mix tank in the mill before discharge to the DTMF (Point C; Figure 1). Two samples of Deilmann tailings (09-E2-GC13 and 09-E2-GC22) were collected from the DTMF at elevations of 395.5 and 377.8 masl in 2009 using a sonic track mounted drill. These samples were discharged to the DTMF prior to 2000[6], and were selected because they contain elevated concentrations of potential

contaminants in the solid samples and distinct Fe concentrations (discussed in section 3.1). These samples had been stored in tightly sealed polyethylene containers in the dark since collection (see Shaw et al.[6] for details).

Because all solids samples were collected in slurry form (solids and liquids), solid phases were separated via pressure filtration (Hazardous Waste Pressure Filter System, Millipore), with a 0.2 μm pore size filter (EMD Millipore Corp.) and N_2 used to pressurize the filter system and a membrane filter. After the aqueous phase was separated and saved for aqueous elemental analysis, the remaining solids were dried at room temperature for 24 h before storage in air-tight bags at 4 °C for geochemical analysis. This procedure was applied to all process samples, final neutralized raffinate samples, and tailings samples investigated.

1.4. Analytical Methods

In most cases, solids samples (composite raffinate, process samples, tailings samples) are dominated by gypsum that precipitates during the neutralization process due to the addition of lime (Ca source) and the presence of H_2SO_4 in the solution raffinate. Because this gypsum interferes with the detection of other mineral phases (data not presented), gypsum was leached by placing dried solid samples in 2 L glass beakers with pure deionized water (Ω = 18 ohms) (S/L ratio of 1:500) and stirring at room temperature for 24 h. Subsequently, the solids and supernatant were separated for analysis via pressure filtration as described above. This was repeated four times until the concentration of dissolved Ca in the filtrate was $\leq$ 100 mg/L, after which the washed solids samples were dried at room temperature for 24 h then gently ground with an agar mortar and pestle. After confirmation with scanning electron microscopy (SEM) that most of the gypsum had been removed from the solids samples (data not shown), subsamples of the dried powdered solids were subjected to

a suite of analyses including inductively coupled plasma mass spectroscopy (ICP-MS), powder X-ray diffraction (XRD), elemental mapping via electron-microprobe analysis (EMPA), transmission electron microscopy (TEM), micro-Raman spectroscopy, and attenuated total reflectance-infrared (ATR-IR) spectroscopy. Unless stated otherwise, all data discussed for solids samples refer to the washed, barium-containing samples from the mill process, the final neutralized raffinate, and the tailings.

Bulk elemental analyses were conducted on subsamples using a Perkin Elmer NexION 300D ICP-MS with a relative standard deviation (RSD) of ±10%. All solids were digested in an acidic media ($HF\text{-}HNO_3$) then left overnight to dissolve. Samples were diluted for analysis of Fe, Al, Mg, and the EOCs Ni, Se, As, and Mo.[25-26]

Powdered subsamples were mounted on the rotating disk transmission holders and bulk X-ray diffractograms measured with an Empyrean Pro PANalytical diffractometer equipped with a cobalt target (Co $K_{\alpha 1}$ radiation, λ = 1.7902 Å), a crystal graphite monochromator, and a scintillation detector. The diffractometer used 40 kV and 45 mA. The scans were measured from 10° to 100° 2θ with a 0.01° step and a scan step time of 85 s. High-resolution synchrotron powder diffraction data for higher sensitivity phase analysis was also collected using beamline 11-BM at the Advanced Photon Source (APS; Argonne, IL) using a wavelength of 0.4587(2) Å.[27] Phase identification and semi-qualitative Rietveld refinement for phase analysis was conducted with XpertHighScore Plus software using the PAN-Inorganic and Mineral Crystal Structure Database, version 1.5. In all cases, the mineral phases used for the analysis (with JCPDS #) were: gypsum (98-000-5396), barite (98-001-1644), ferrihydrite (98-011-1017), hydrotalcite (98-000-6182 and 98-004-0925), calcite (98-000-5314), magnesium calcite (98-004-1760), brucite (98-001-1718), gibbsite (98-000-5450), diaspore (98-00-5681), bayerite (98-001-1683), boehmite (98-000-6538), corundum (98-005316), periclase

(98-000-5907), and magnesium peroxide (98-001-4869). The qualitative Rietveld phase analysis conducted with the XpertHighScore Plus software was tested for validity by analyzing a reagent grade goethite standard (Fisher Scientific) and an unwashed raffinate product (known to show only gypsum[28]) and matching the XRD data with unlikely multiple phases with diffraction peaks in all regions. Rietveld analysis (accuracy of $\leq 10\%$) confirmed that goethite and gypsum were the major phases present.

Subsamples were placed in cylindrical plugs (5 mm diameter), filled with epoxy, and allowed to harden at room temperature. The surfaces of the plugs were then polished for microanalysis with EMPA using a JEOL JXA-8900L operating at 15 kV and 20 mA, with a beam size of 2 μm and counting time of 20 s. Two distinct 60×60 μm areas were analyzed and mapped for Fe, As, Mo, Se, Ni, Al, and Mg in each plug to obtain a representative mapping of the phase(s) of interest. For all samples mapped, a preliminary rapid scan was performed to determine which EOCs (e.g., As, Ni, Mo, Se) could be observed before undertaking more detailed mapping. In cases where the concentration of the element of interest was too low to observe (signal = background), detailed mapping was not undertaken.

TEM imaging and analysis were conducted on selected particles in the subsamples via energy dispersive X-ray analysis (EDX) and electron diffraction (ED) using a Philips CM-200 microscope operating at 200 kV. Subsamples were prepared by dropping dilute solutions of the particles in ethanol onto 400-mesh carbon-coated copper grids and evaporating the solvent to dryness before inserting them into the sample holder and chamber.

Raman spectra were collected on subsamples with a Renishaw InVia Raman microscope in both normal and confocal mode. Laser excitation was provided by a solid state diode near-IR laser operating at 785 nm. The laser beam produced a spot size of approximately ≤ 5 μm in diameter using

the 50× short distance objective. The average of five scans collected from 1400 to 150 cm^{-1} is reported. The energy resolution was 4 cm^{-1} at the full width half maximum (FWHM) of the internal Si reference peak. Scans were collected at 30 s per scan using 10% of the laser output at the microscope exit to avoid radiation damage to the ferrihydrite particles.[29] Infrared spectra were obtained on powdered subsamples using a Perkin Elmer Fourier transform infrared (FTIR) (Spectrum BX model) spectrometer with a Miracle single bounce diamond ATR cell from PIKE Technologies. Spectra over the 4000-550 cm^{-1} range were obtained by the co-addition of 200 scans with a resolution of 4 cm^{-1} at the FWHM of the strongest C-H vibration of the internal polystyrene standard.

1.5. Thermodynamic Modeling

Thermodynamic modeling was used to simulate the precipitation of secondary mineral phases of Mg, Al, and Fe in the mill during a step-wise neutralization of the raffinate solution (pH 1 to the terminal pH of 10.5 at 0.5 pH steps) with slaked lime. All modeling calculations were performed using PHREEQC, version 2.18.3.5570.[30] The Lawrence Livermore National Laboratory (LLNL) thermodynamic database (included with PHREEQC) modified with additional thermodynamic data (see previous similar computations[6,9]) as well as hydrotalcite thermodynamic data from the HATCHES (HArwell/Nirex Thermodynamic Database for CHemical Equilibrium Studies) Database - version NEA19 (i.e., reaction $Mg_4Al_2O_{17}H_{20} + 14H^+ = 2Al^{+3} + 17H_2O + 4Mg^{+2}$; Log k = 75.34).[31]

2. FIGURES

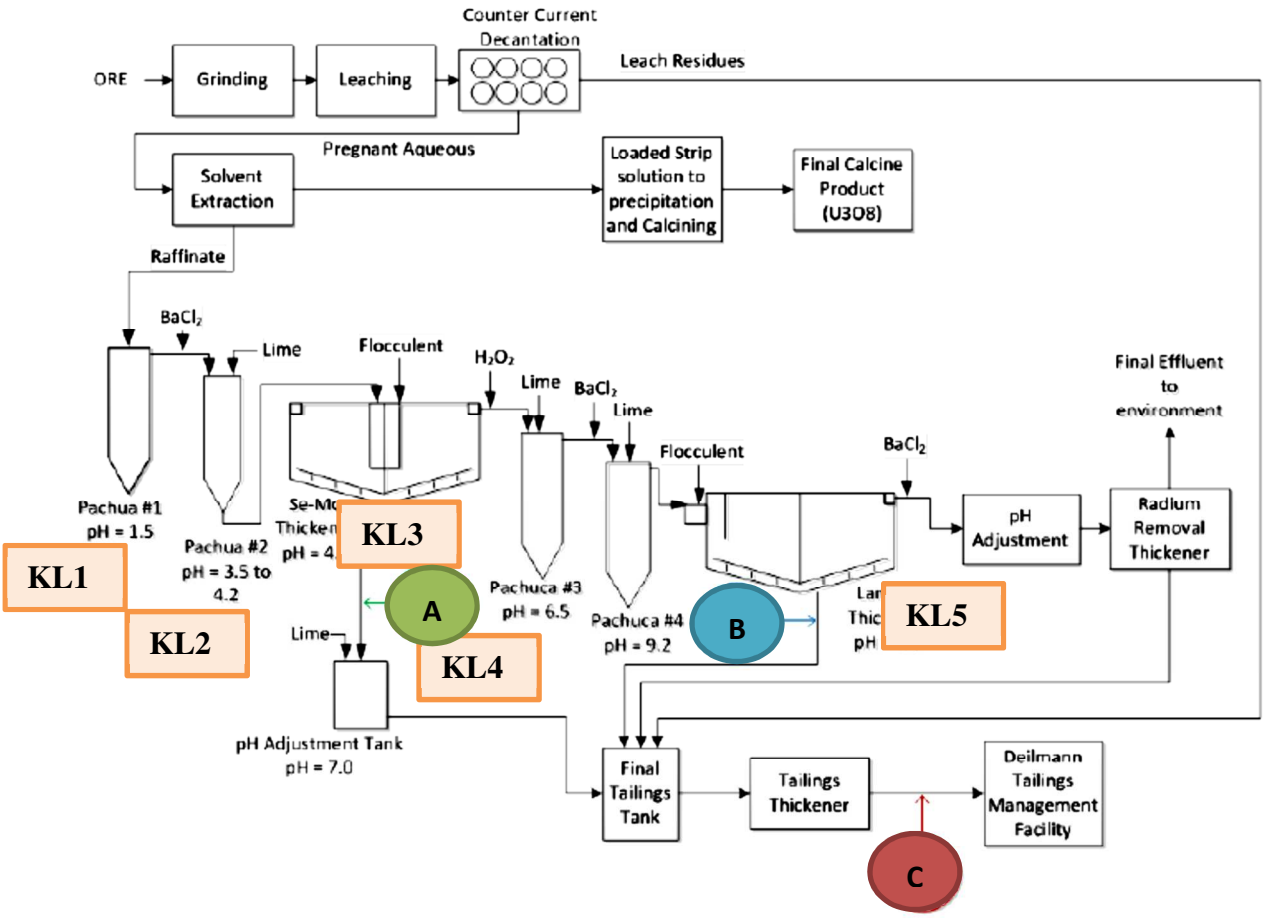

Figure S0. Schematic diagram of the Key Lake Mill neutralization process currently employed on the McArthur uranium ores. The sampling points in the process are identified by alphanumeric identifiers. These samples are the neutralized raffinate (A), underflow tailings (B) (which make up the 11-CS-Ba composite), the fresh tailings sample (11-McTail-01) (C), and different steps in the process (KL1 to KL5).

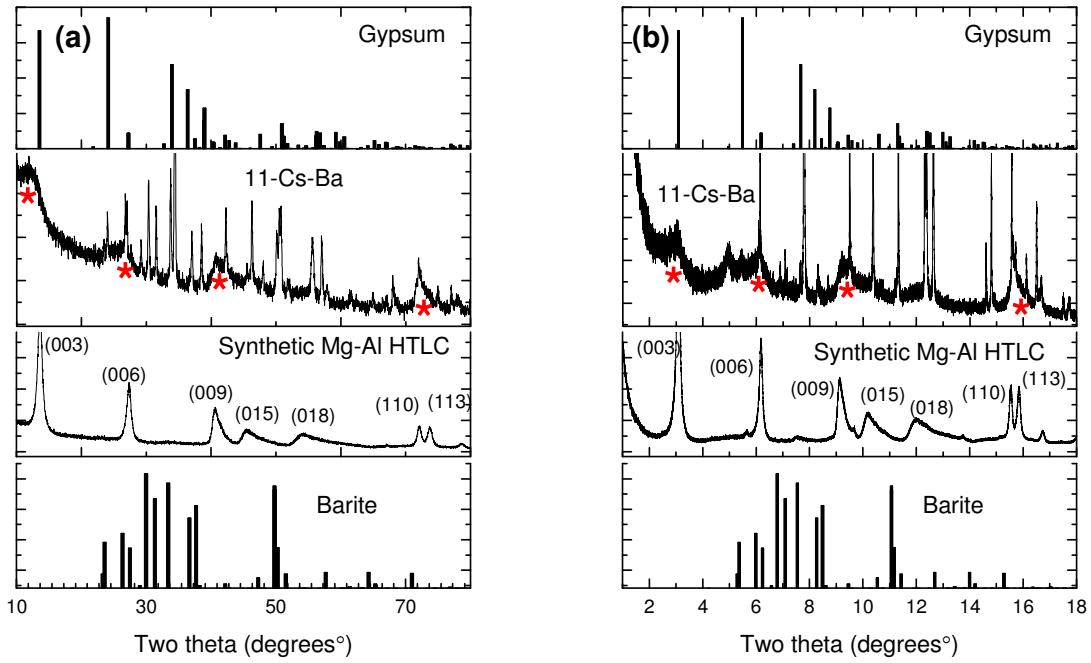

Figure S1. Powder XRD analyses using (a) lab- (Co K_α λ =1.70 Å) and (b) synchrotron-based sources (λ =0.41 Å) on the final neutralized raffinate (11-Cs-Ba) as well as relevant synthetic phases of interest (gypsum, barite, and Mg-Al hydrotalcite (Mg-Al HTLC)). From the lab-based XRD analyses, the presence of the Mg-Al HTLC was observed via sample comparison to the synthetic Mg-Al HTLC phase; however, the presence of barite and residual gypsum resulted in some interference. For the synchrotron-based XRD analyses, the presence of Mg-Al HTLC and its characteristic planes (e.g. (003), (006), (009), (110), (113)) in the final neutralized raffinate are observed. Under each of the raffinate data we have placed an * to indicate these peaks to be a contribution from the hydrotalcite phase to the overall XRD data.

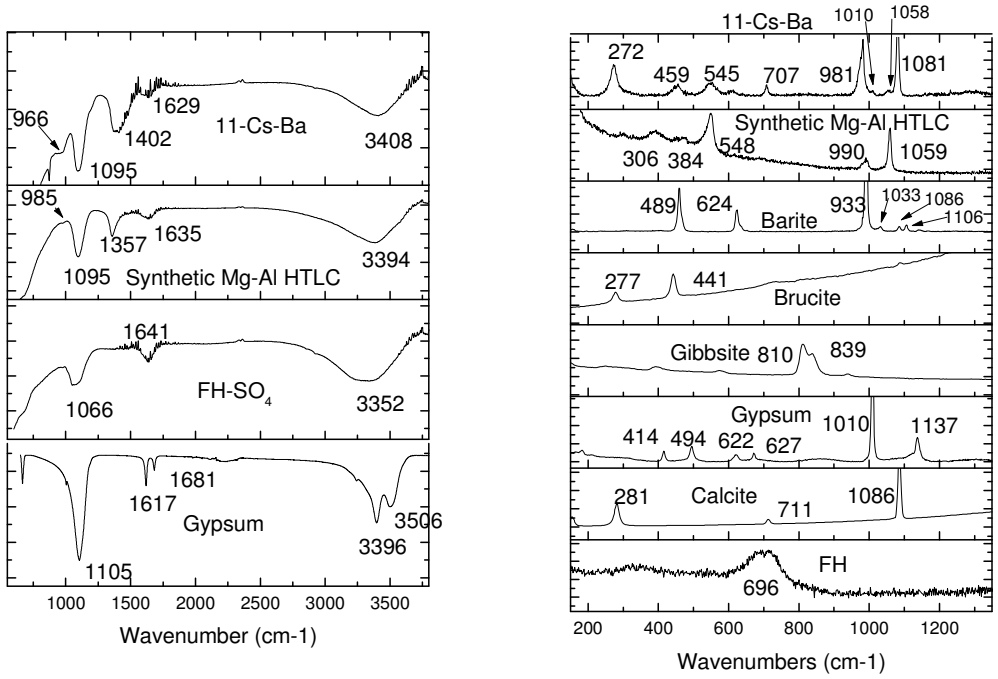

Figure S2. ATR-IR and micro-Raman spectra of the final neutralized raffinate (11-Cs-Ba) compared to the relevant phases of interest. The ATR-IR spectra show the final neutralized raffinate sample is composed of a metal-containing hydrated hydroxyl sulfate carbonate phase unlike that of the expected phases (e.g., ferrihydrite, gypsum, barite) but which matched quite well with Mg-Al hydrotalcite. Micro-Raman spectra of the final neutralized raffinate similarly shows a molecular signal in agreement with Mg-Al hydrotalcite and unlike that of the expected Mg or Al hydroxide (e.g. gibbsite, brucite) and other phases (calcite, ferrihydrite-FH gypsum, barite).

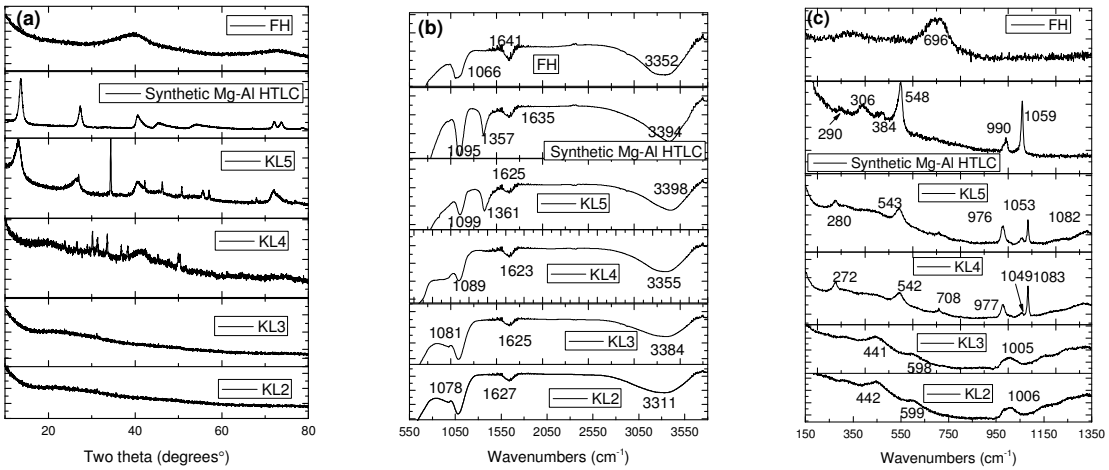

Figure S3.(a) Powder XRD (Co K_α λ =1.70 Å), (b) ATR-IR, and (c) Raman spectra of Key Lake process samples (11-KL-02 to 11-KL-05) compared to synthetic Mg-Al hydrotalcites (Mg-Al HTLC) and ferrihydrite (FH) .

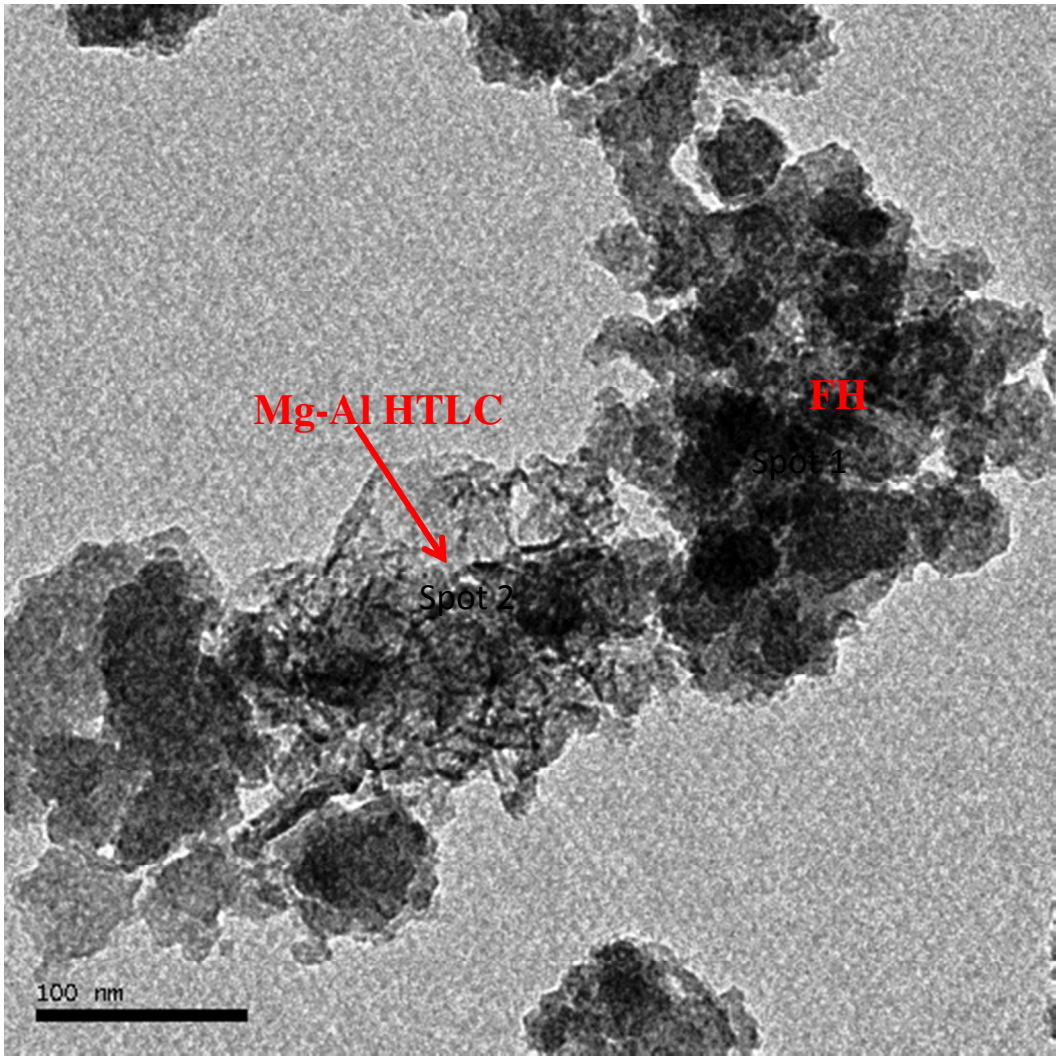
Mg-Al HTLC
FH
Spot 1
Spot 2
100 nm

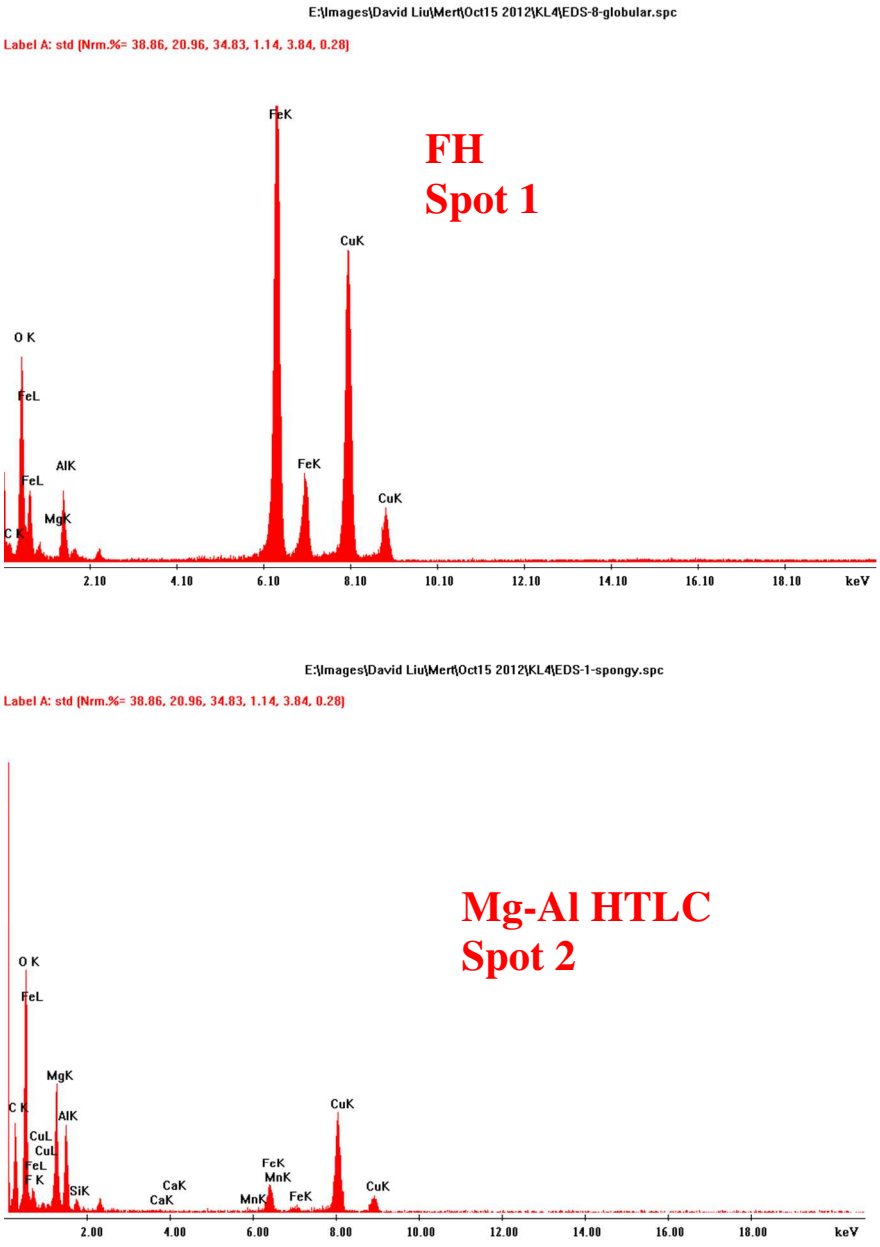

Figure S4. TEM and EDX analysis of a selected particle that showed both ferrihydrite and Mg-Al hydrotalcite association in the Key Lake mill neutralization process at pH 6.4 (sample 11-KL-04). Spot 1 in the EDX spectra shows an iron-rich phase as observed for ferrihydrite, while spot 2 shows our typically observed Mg-Al hydrotalcite. The first observation of the Mg-Al hydrotalcite component occurred at this pH 6.4 step and, as such, we chose the corresponding sample to see if the close association observed in the final neutralized raffinate sample (see Figure 4) could be detected. This is indeed observable in this image at the formation step of Mg-Al hydrotalcite in the milling process, providing further evidence of its close association with ferrihydrite.

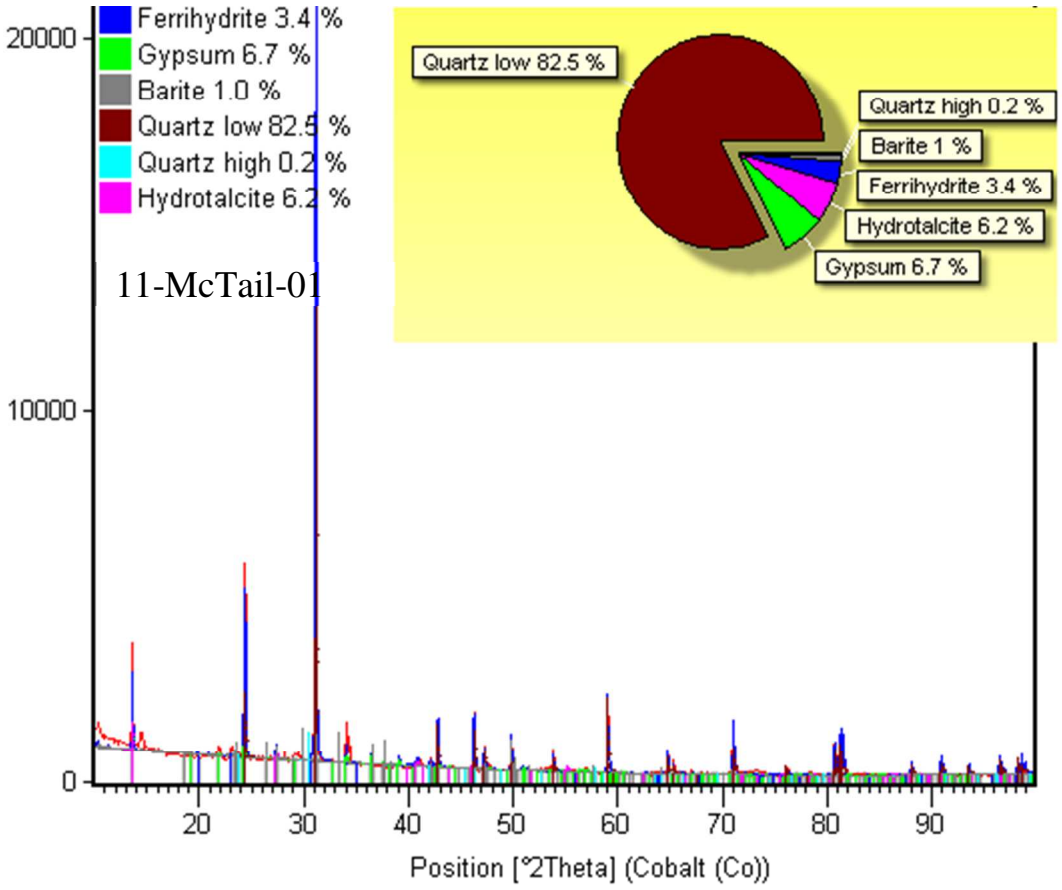
Ferrihydrite 3.4 %
Gypsum 6.7 %
Barite 1.0 %
Quartz low 82.5 %
Quartz high 0.2 %
Hydrotalcite 6.2 %
11-McTail-01
Quartz low 82.5 %
Quartz high 0.2 %
Barite 1 %
Ferrihydrite 3.4 %
Hydrotalcite 6.2 %
Gypsum 6.7 %
20000
10000
0
20
30
40
50
60
70
80
90
Position [°2Theta] (Cobalt (Co))

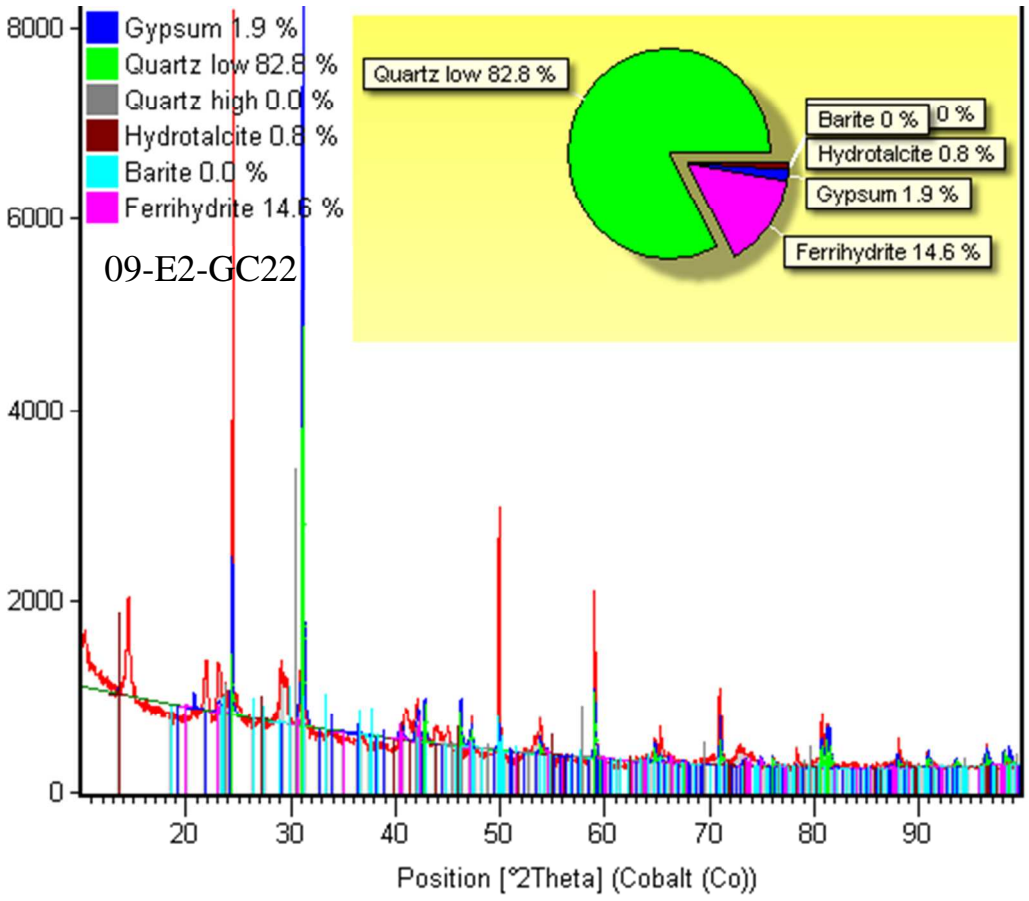
Gypsum 1.9 %
Quartz low 82.8 %
Quartz high 0.0 %
Hydrotalcite 0.8 %
Barite 0.0 %
Ferrihydrite 14.6 %
09-E2-GC22
Quartz low 82.8 %
Barite 0 %
Hydrotalcite 0.8 %
Gypsum 1.9 %
Ferrihydrite 14.6 %
8000
6000
4000
2000
0
20
30
40
50
60
70
80
90
Position [°2Theta] (Cobalt (Co))

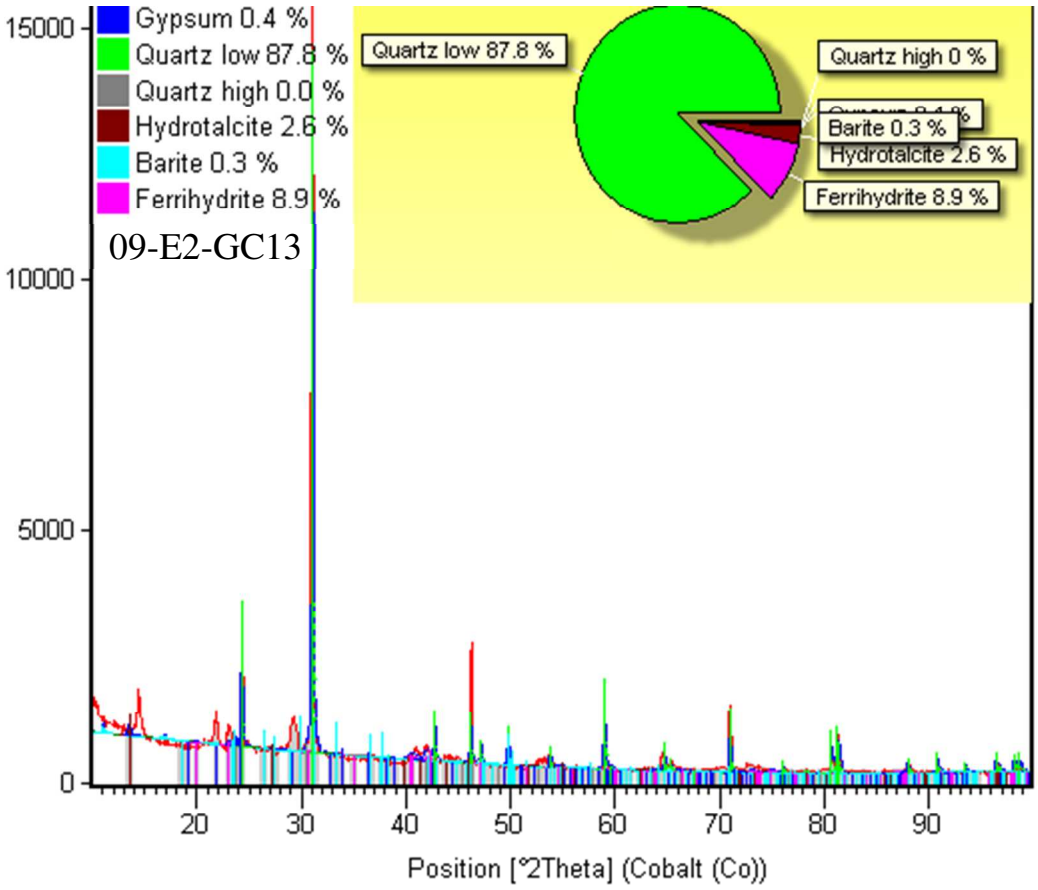

GC13

Figure S5. XRD (Co K_α λ =1.70 Å) of tailings samples from McArthur (11-McTail-01) and Deilmann (09-E2-GC13 and 09-E2-GC22) tailings samples from the Key Lake mill and the Dielmann Tailings Management Facility. The qualitative XRD Rietveld phase analysis of these samples using XperhighScore Plus shows a large amount of quartz as well as other phases of interest (e.g., ferrihydrite, barite, gypsum), including Mg-Al hydrotalcite.

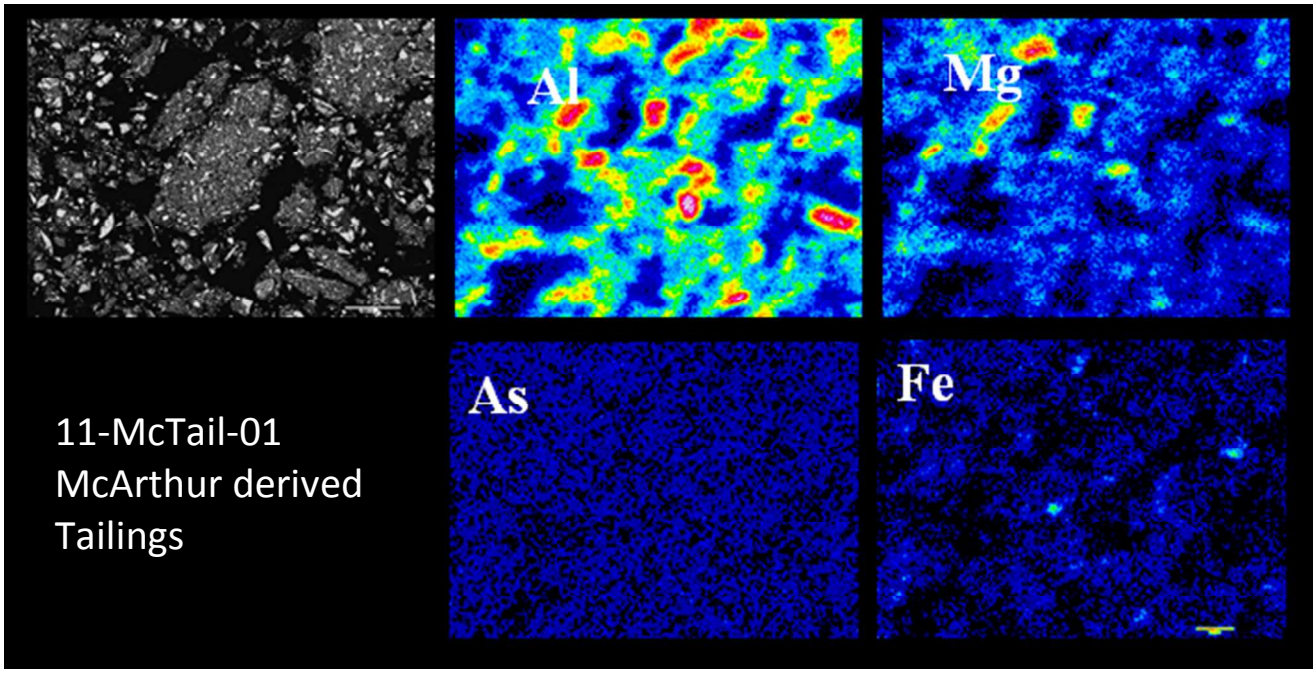

11-McTail-01
McArthur derived
Tailings

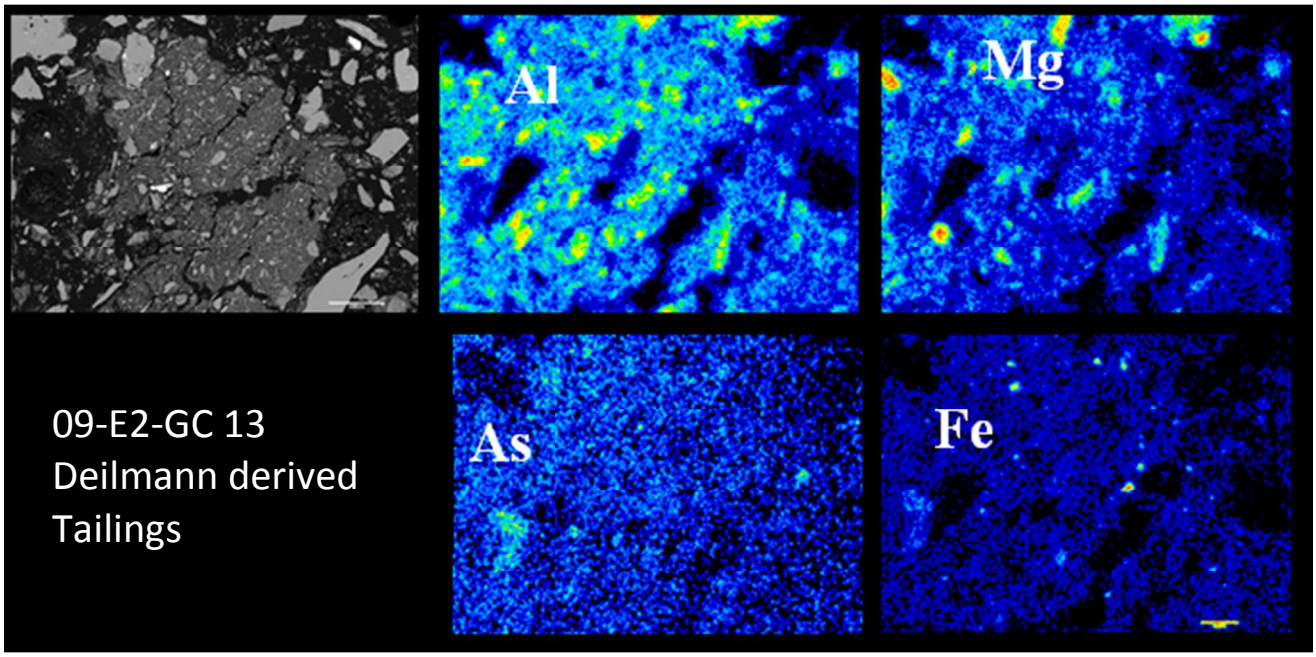

09-E2-GC 13
Deilmann derived
Tailings

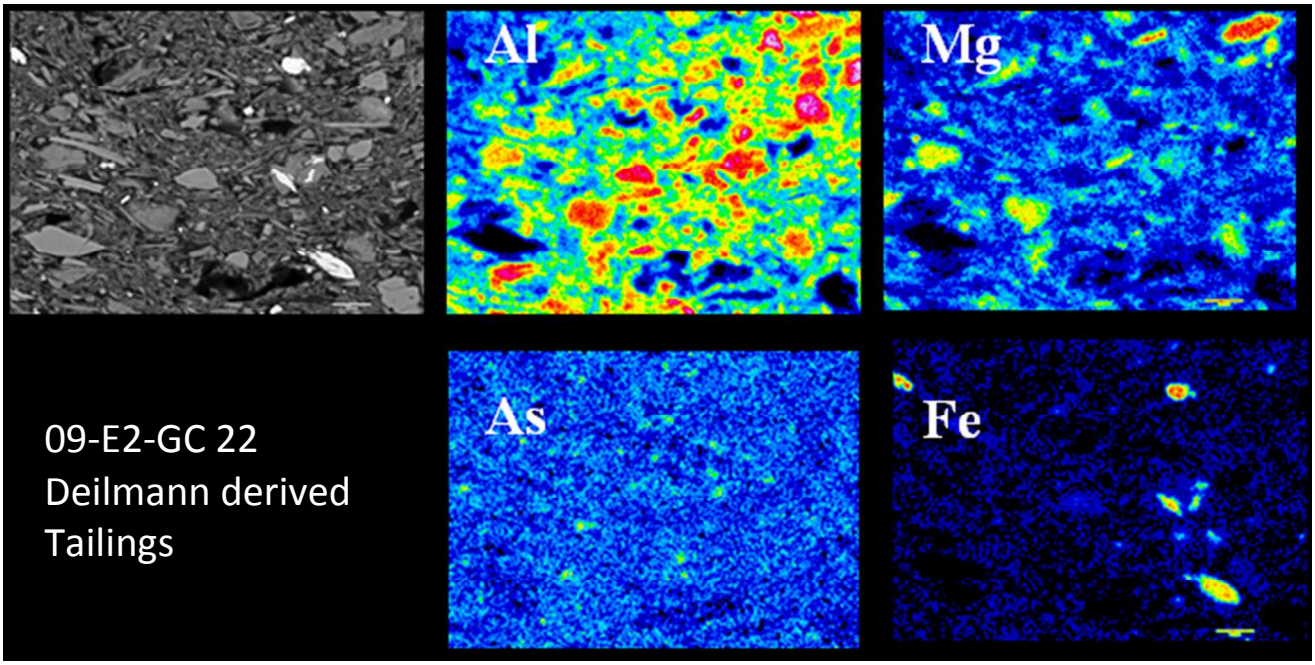

Figure S6. EMP maps of elements of interest in the neutralized gypsum washed tailings products from (a) McArthur river tailings (sample 11-McTail-01), (b) Deilmann tailings sample 09-E2-GC 13, and (c) Deilmann tailings sample 09-E2-GC 22. The Al and Mg are homogeneously distributed and correlated throughout the sample. Iron is also spatially correlated with Mg and Al. The As observed in the Deilmann samples (09-E2-GC 22 and 09-E2-GC 13) correlates spatially with Fe as well as Al and Mg. For the McArthur river tailings, the As concentration is too low to be clearly observed. Interestingly, various hot spots are evident for the various tailings samples for Fe, Al, and Mg. These hot spots result from the contribution of secondary minerals (ferrihydrite and Mg-Al hydrotalcite) but also primary minerals (pyrite, silicates, hydroxides) present in the tailings samples as a result of incomplete dissolution (see Figures 1 and 2). Scale bar, 100 µm.

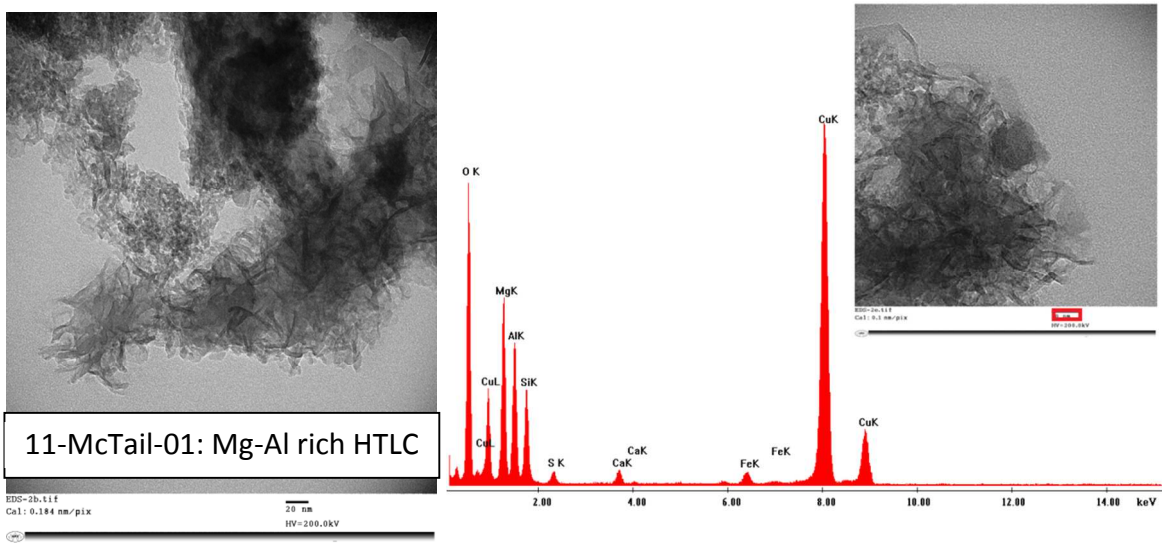
11-McTail-01: Mg-Al rich HTLC
EDS-2b.tif
Cal: 0.184 nm/pix
20 nm
HV=200.0kV
O K
MgK
AlK
SiK
CuL
CuL
S K
CaK
CaK
FeK
FeK
CuK
CuK
2.00
4.00
6.00
8.00
10.00
12.00
14.00
keV

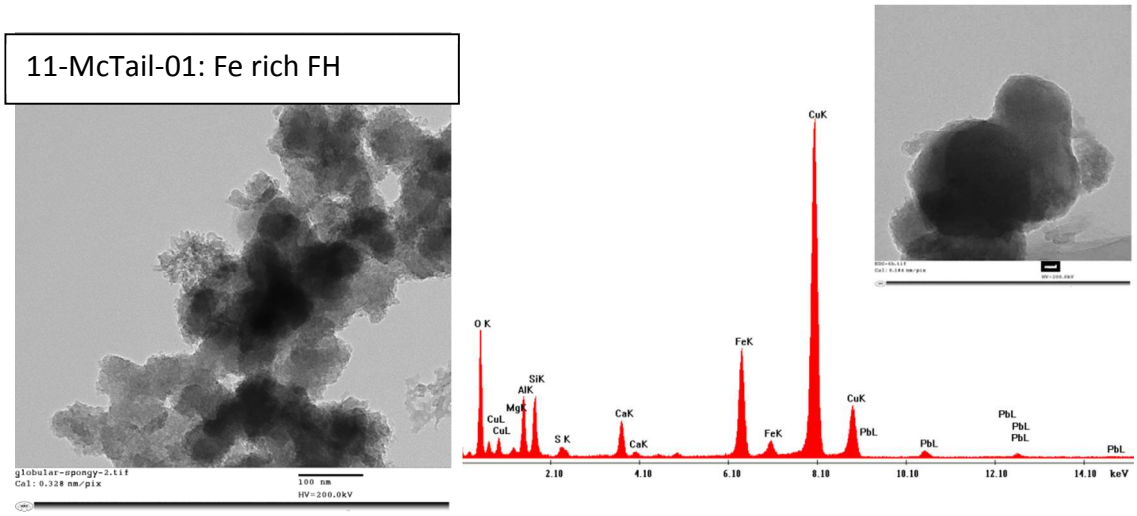
11-McTail-01: Fe rich FH
globular-spongy-2.tif
Cal: 0.328 nm/pix
100 nm
HV=200.0kV
O K
CuL
CuL
MgK
AlK
SiK
S K
CaK
CaK
FeK
FeK
CuK
CuK
PbL
PbL
PbL
PbL
PbL
2.10
4.10
6.10
8.10
10.10
12.10
14.10
keV

09-E2-GC13: Mg-Al rich HTLC

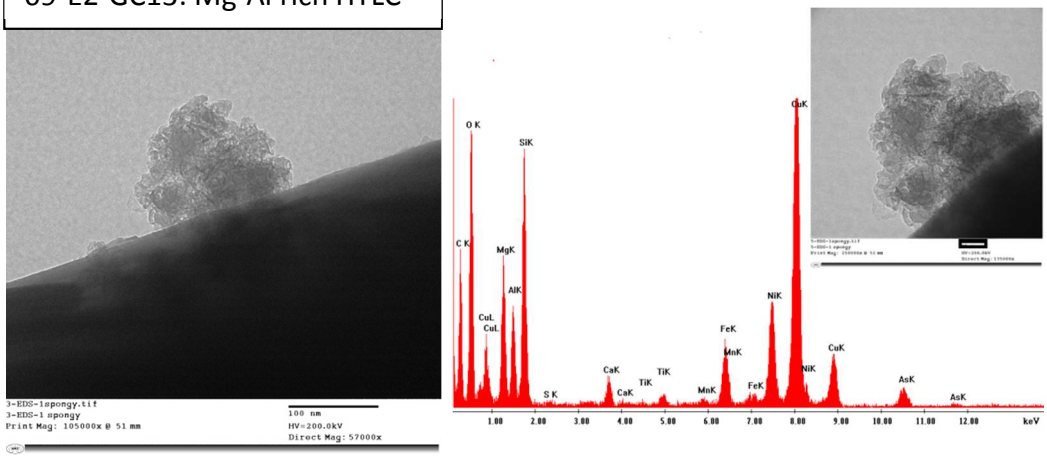

09-E2-GC13: Fe rich FH

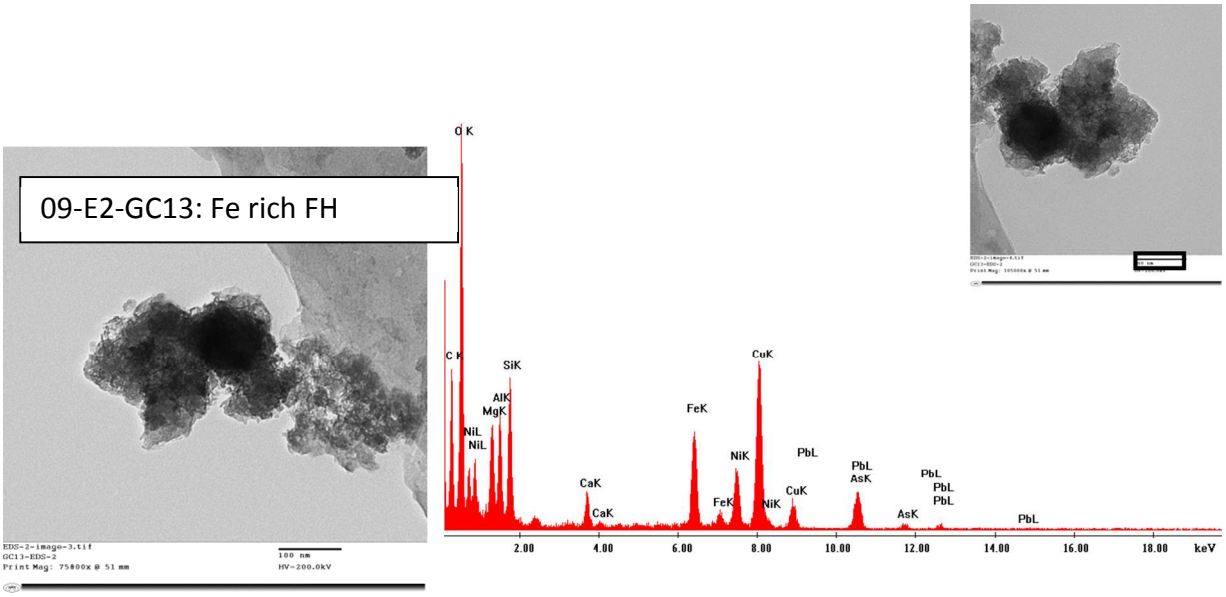

09-E2-GC22: Fe rich FH

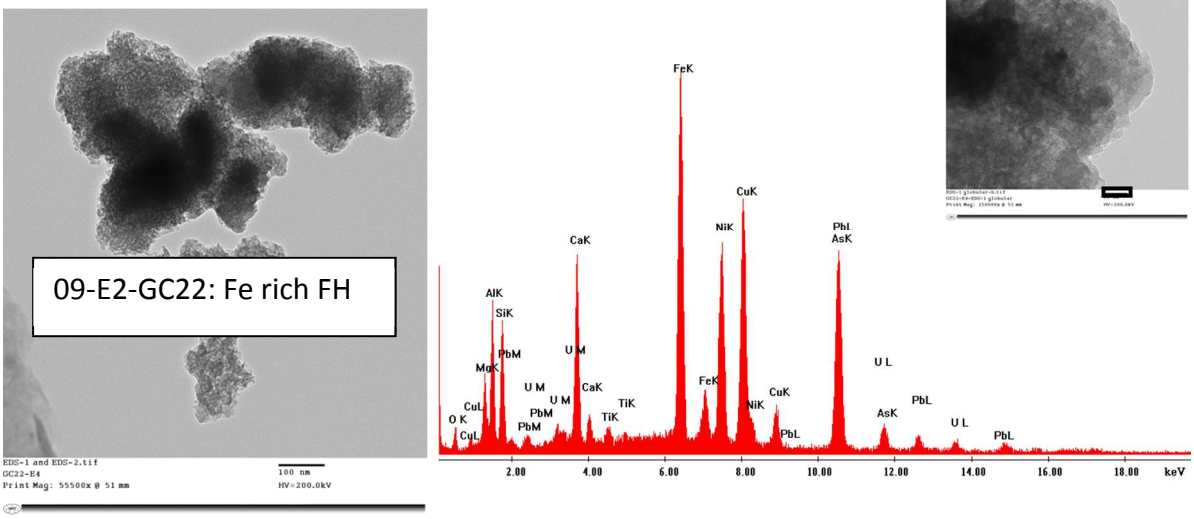

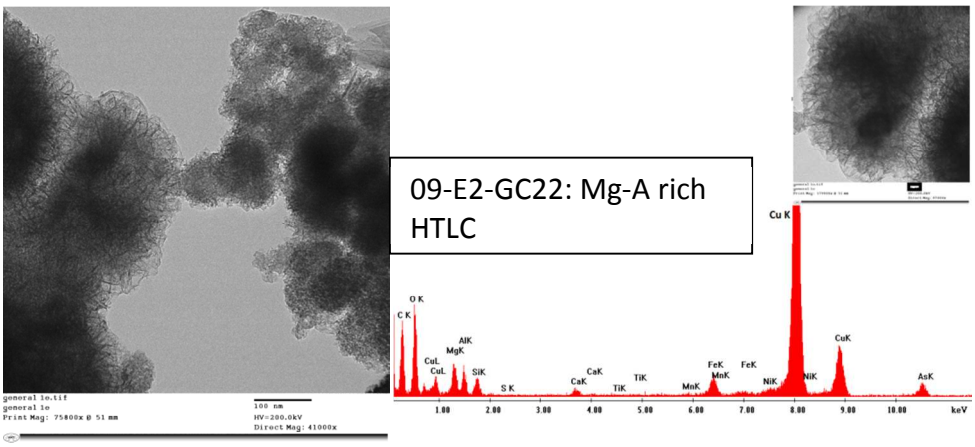

Figure S7. TEM and corresponding EDX analysis of common particles found throughout McArthur and Deilmann (09-E2-GC13 and 09-E2-GC22) tailings samples. These data show the two types of particles found widely distributed throughout the tailings: the iron rich globular ferrihydrite particles and the Mg-Al rich hydrotalcite.

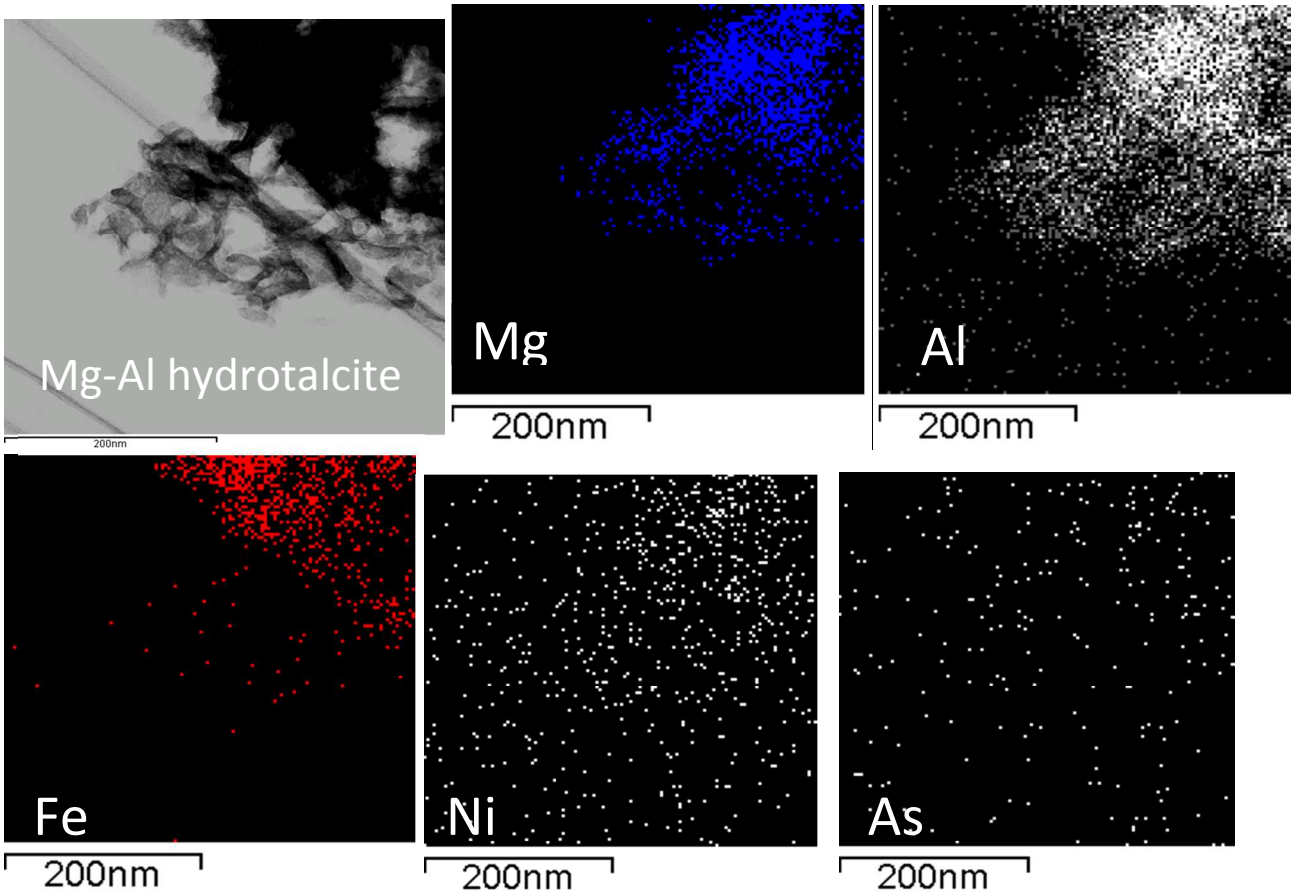
Mg-Al hydrotalcite
200nm
Mg
200nm
Al
200nm
Fe
200nm
Ni
200nm
As
200nm

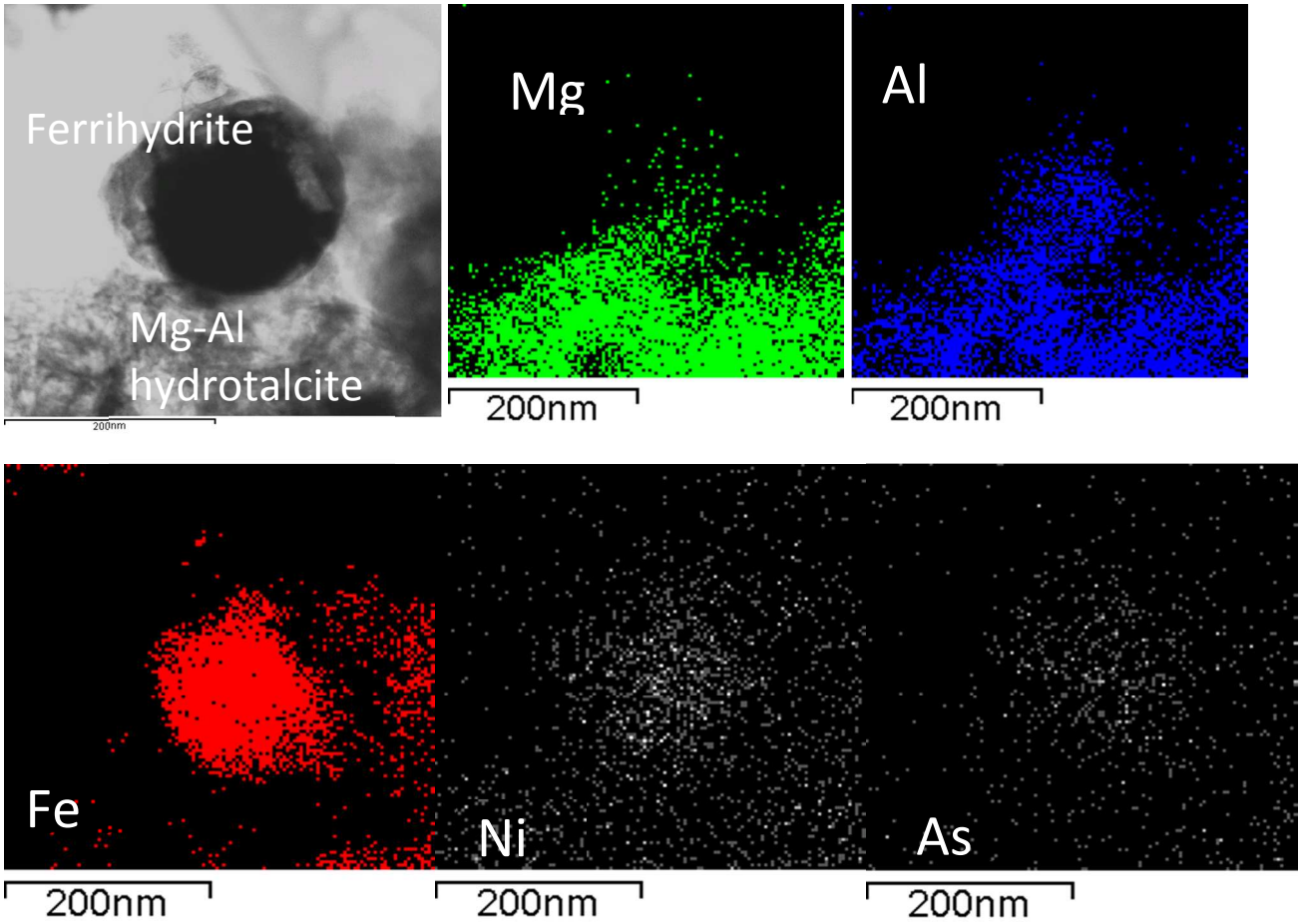

Figure S8. STEM images and elemental mapping of both nanoparticles (ferrihydrite and Mg-Al hydrotalcite) found in the final neutralized raffinate [11-Cs-Ba] are presented. From these images and corresponding elemental mapping we can see the spatial correlation at the nano-scale of the individual phases. In case of the hydrotalcite the Mg and Al are correlated with the sponge like phase but in addition the presence of Fe in the hydrotalcite particles is also observed. In case of the ferrihydrite nano-particles, the presence of iron is naturally observed but interesting the presence of Al and some Mg is also observed. It should be noted that the McArthur tailing (11-McTail-01) was not analyzed as the sample (a) was too low to detect the As and Ni mapping areas.

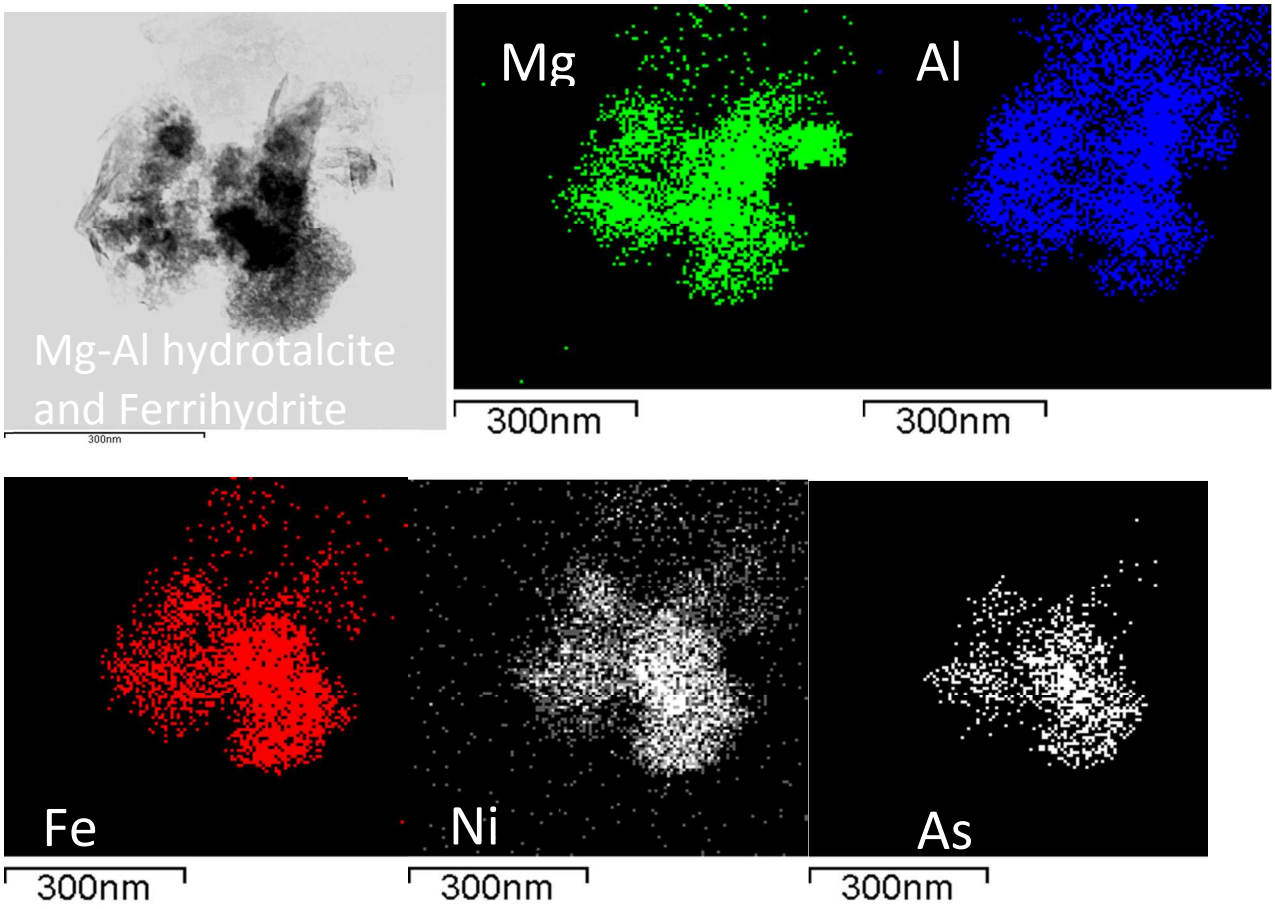
Mg-Al hydrotalcite and Ferrihydrite
300nm
Mg
Al
300nm
300nm
Fe
Ni
As
300nm
300nm
300nm

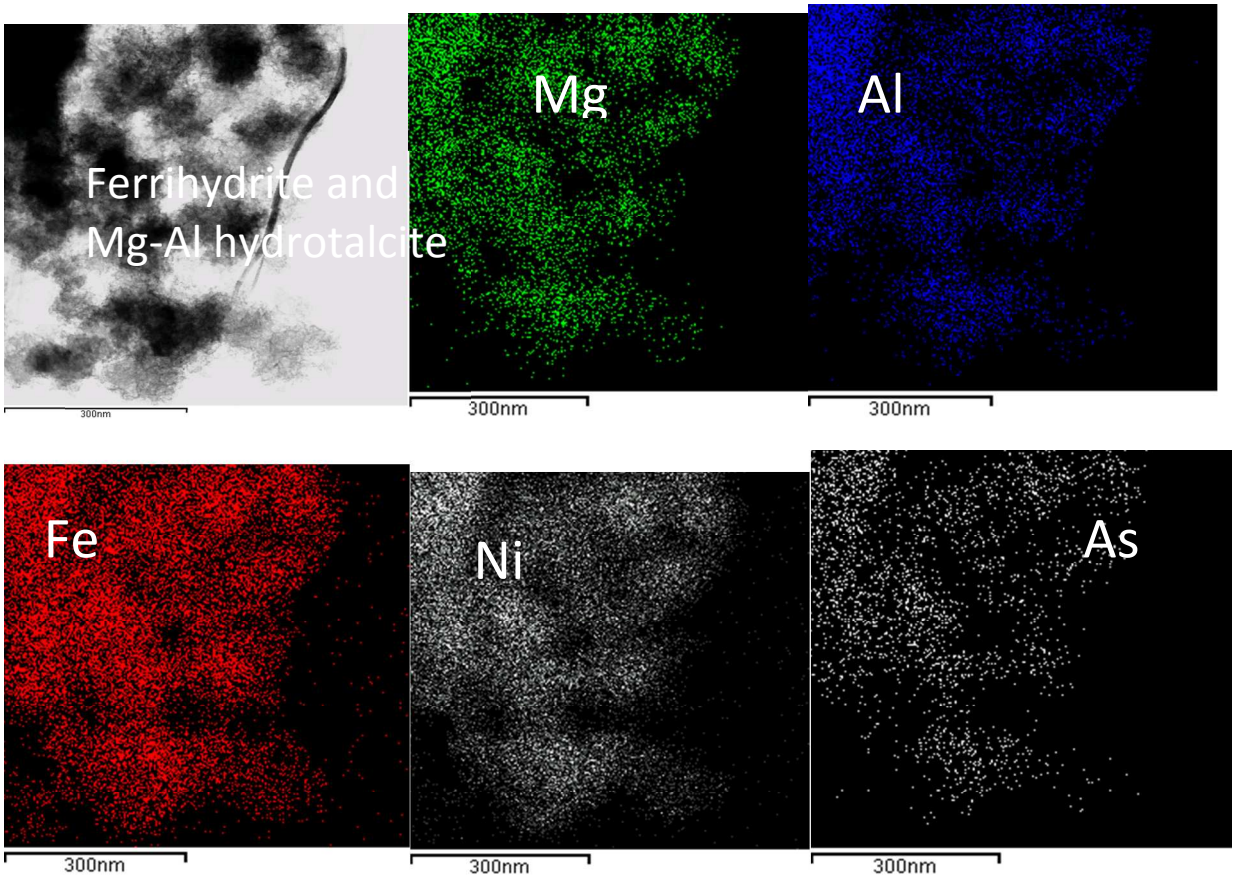

Figure S9. STEM images and elemental mapping of both nanoparticles (ferrihydrite and Mg-Al hydrotalcite) found in the Deilmann tailings samples. From these images we can see the spatial correlation at the nano-scale of the individual phases. In the case of the hydrotalcite nano-particles, we can see the Mg-Al correlation with some Fe but also in this case the presence of both Ni and As are observed indicating that they are present with the hydrotalcite phase. In the case of the ferrihydrite nano-particles, the elemental nano mapping showed Fe associated with it as well as some Al, Ni and As.

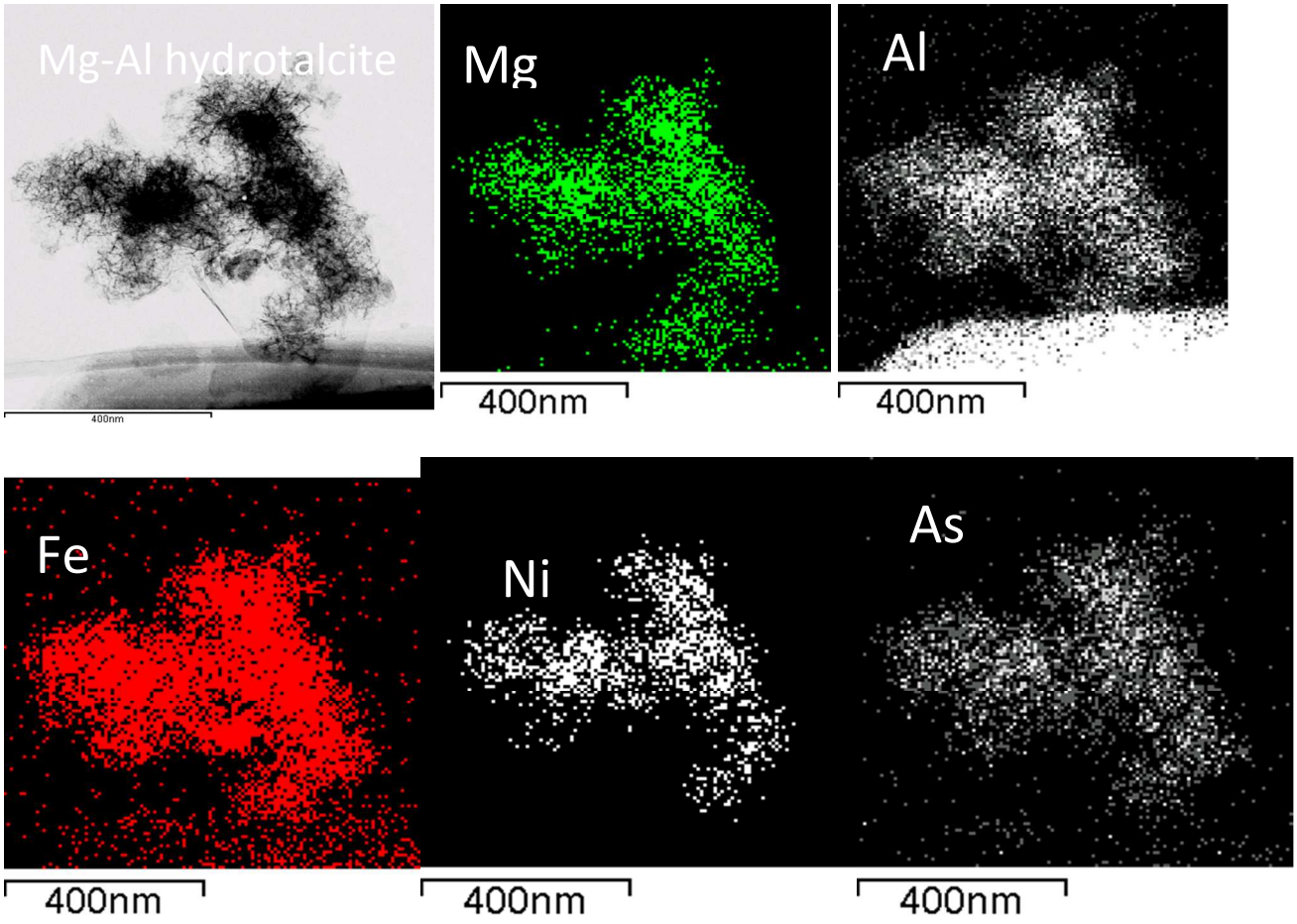
Mg-Al hydrotalcite
400nm
Mg
400nm
Al
400nm
Fe
400nm
Ni
400nm
As
400nm

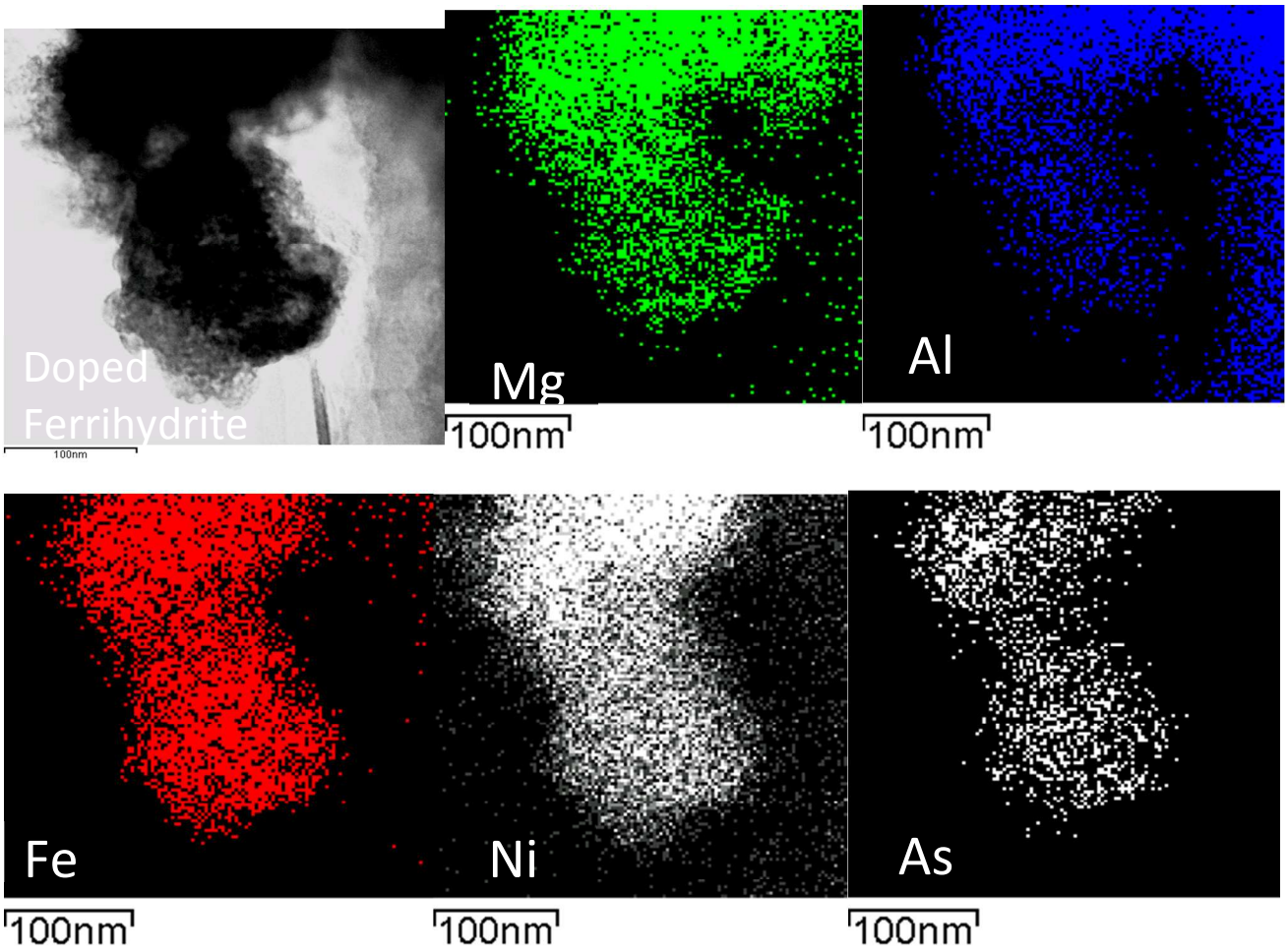

Figure S10. STEM images and elemental mapping of both nanoparticles (ferrihydrite and Mg-Al hydrotalcite) found in the Deilmann 09-E2-GC22 tailings samples. From these images we can see the spatial correlation at the nano-scale of the individual phases. For the hydrotalcite nano-particles, again a Mg-Al correlation with Fe is observed but also in this case the presence of both Ni and As are observed with the hydrotalcite phase. In the case of the ferrihydrite nano-particles, the elemental nano mapping showed Fe associated with it as well as Al, Ni and As.

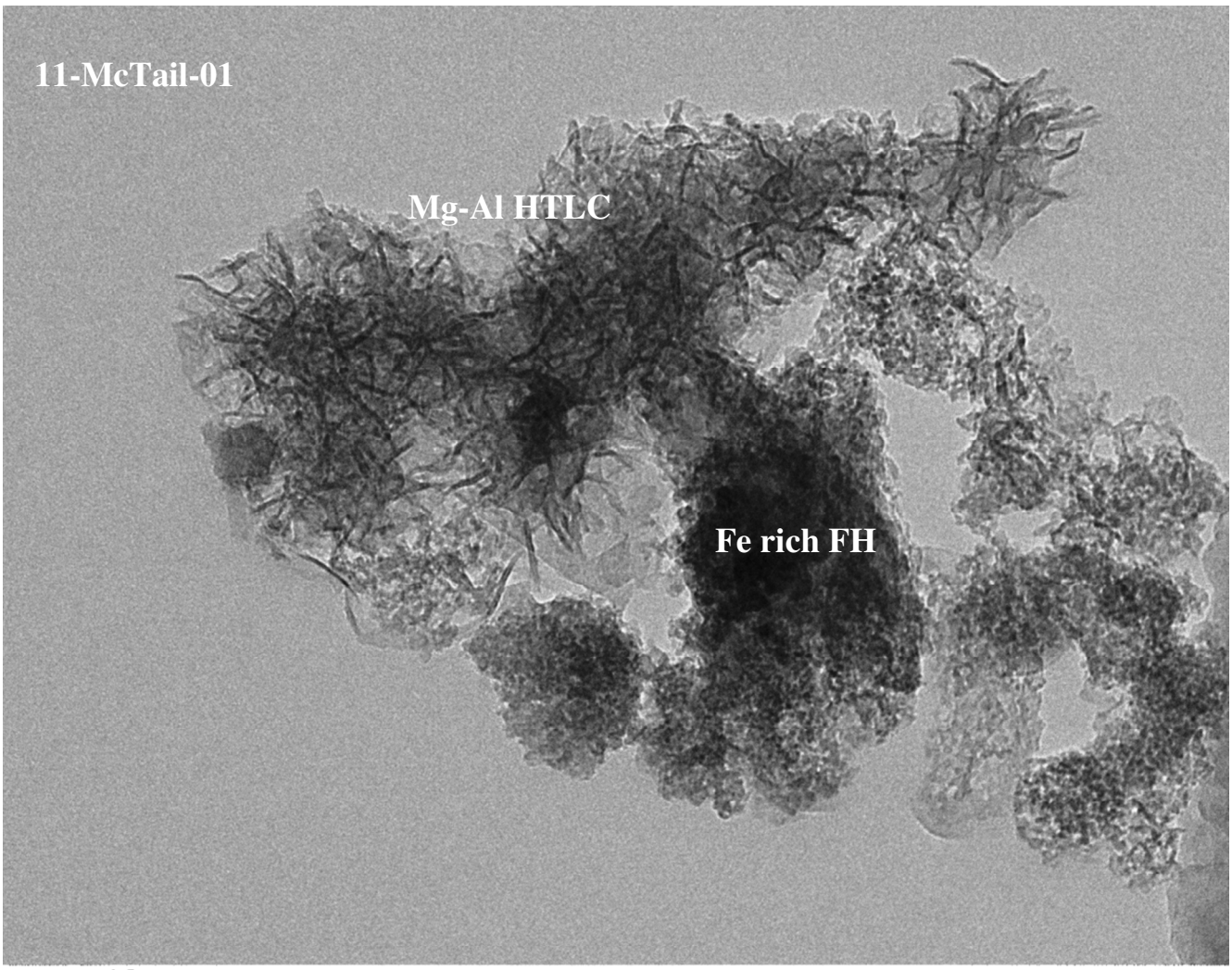
11-McTail-01
Mg-Al HTLC
Fe rich FH
EDS-2.tif
Cal: 0.328 nm/pix
100 nm
HV=200.0kV

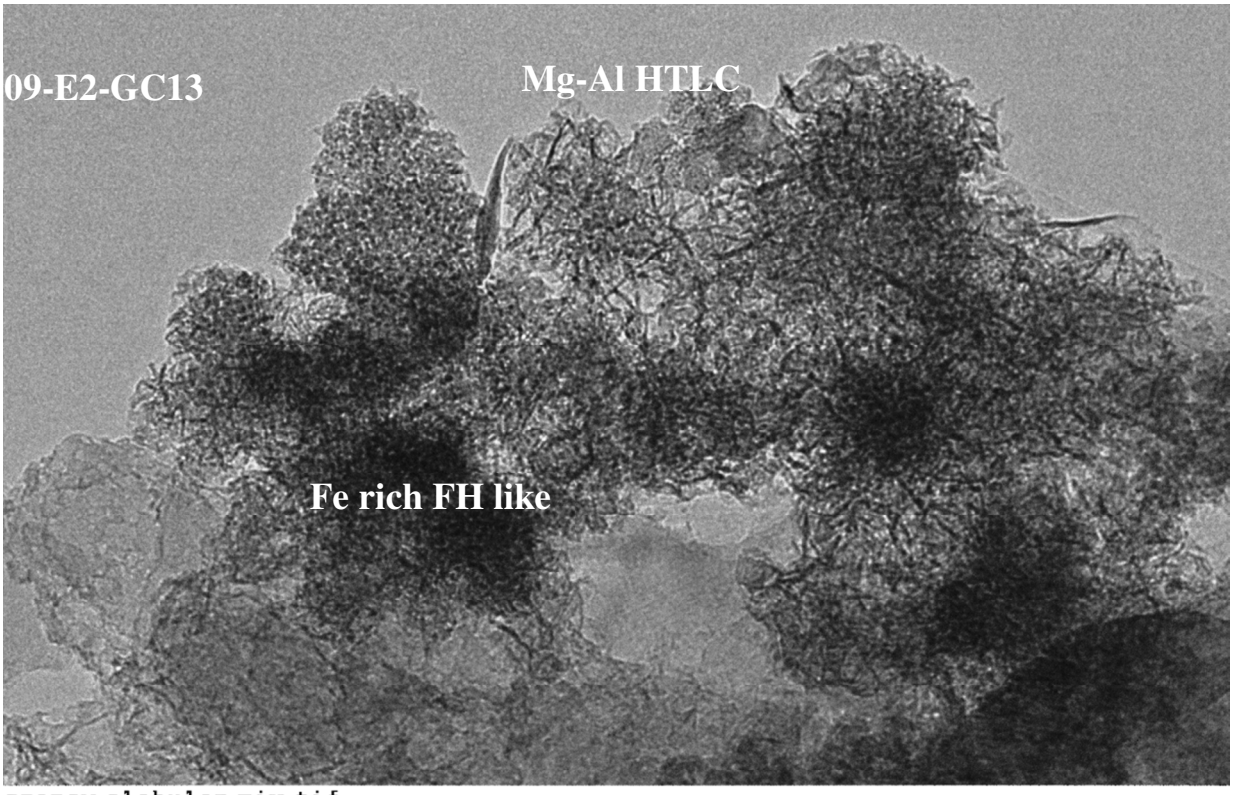

spongy globular mix.tif
spongy-globular mix
Print Mag: 75800x @ 51 mm

100 nm
HV=200.0kV
Direct Mag: 41000x

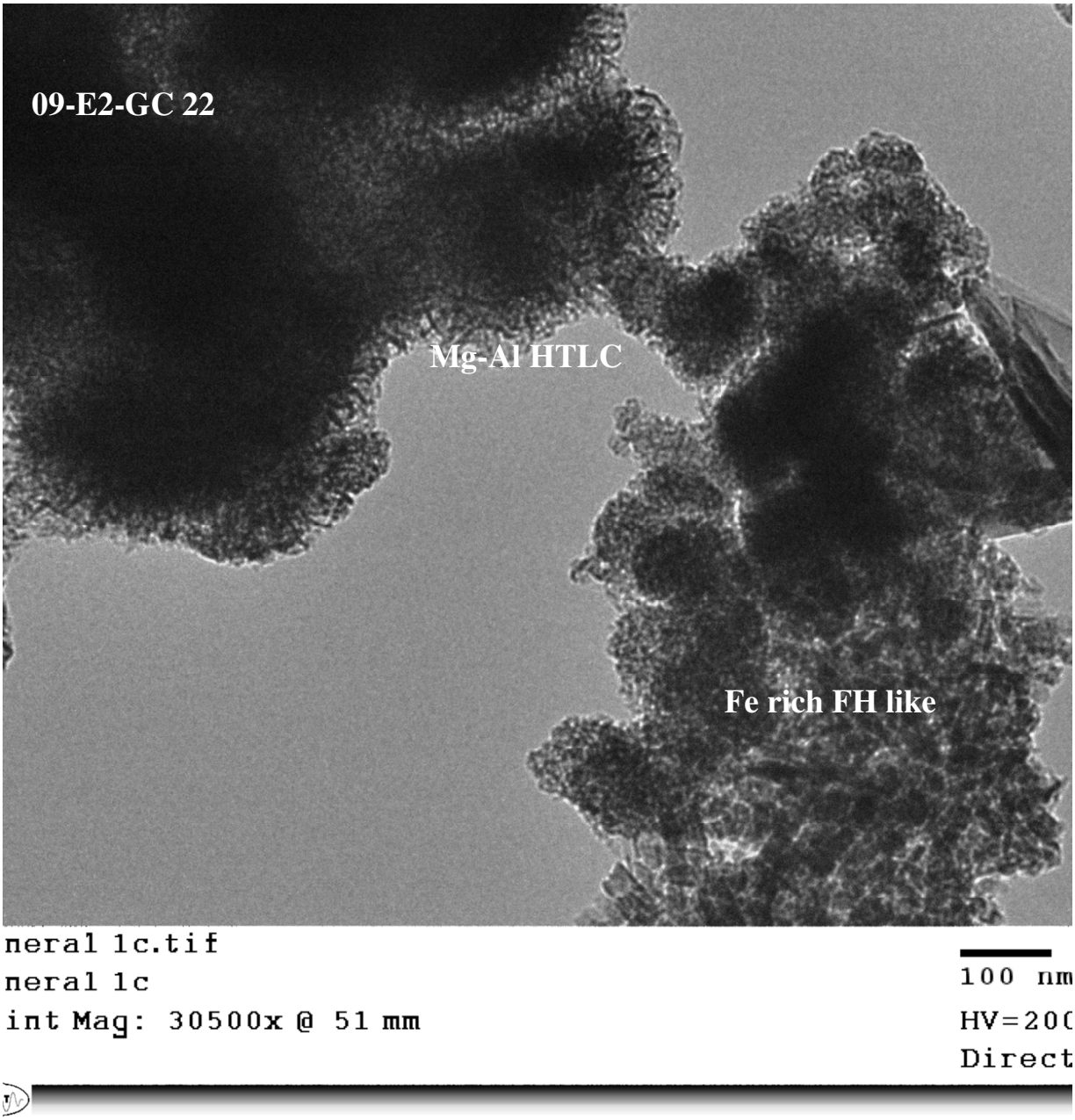

Figure S11. TEM images of particles present in the gypsum washed McArthur 11-McTail-01, Deilmann 09-E2-GC13, and Deilmann 09-E2-GC22 samples. These images show the close association of both globular (ferrihydrite) and spongy (Mg-Al) particles.